Editors' Suggestion

Band-gap discontinuity in semiconductor alloys with dissimilar wavefunction characters at the band edges

Xuefen Cai [1,2] Su-Huai Wei [3,*] Peter Deák,[3] Jingxiu Yang,[4] Chen Zhang,[2] Bin Wang,[1]
Shu-Shen Li,[2] and Hui-Xiong Deng[2,†]

[1] *State Key Laboratory of Radio Frequency Heterogeneous Integration (Shenzhen University), College of Physics and Optoelectronic Engineering, Shenzhen University, Shenzhen 518060, China*

[2] *State Key Laboratory of Superlattices and Microstructures, Institute of Semiconductors, Chinese Academy of Sciences, Beijing 100083, China*

[3] *Beijing Computational Science Research Center, Beijing 100193, China*

[4] *Key Laboratory for Comprehensive Energy Saving of Cold Regions Architecture of Ministry of Education, School of Materials Science and Engineering, Jilin Jianzhu University, Changchun 130118, China*

(Received 19 January 2024; accepted 20 May 2024; published 5 June 2024)

Forming a semiconductor alloy is a common practice to extend material properties for specific applications. While empirical continuous rules have been proposed and extensively validated to predict property changes in conventional alloys, there are certain isovalent alloys that exhibit discontinuous variations in electronic structures, defying the application of established rules. However, the underlying cause of this phenomenon has not been clearly stated. Through rigorous first-principles calculations on a prototypical α-$(Rh_xGa_{1-x})_2O_3$ alloy, we find a steplike, discontinuous variation in the band gap. A thorough examination reveals that this is correlated with the unconventional evolution of wavefunction characters at the band edges and the associated wavefunction localization on the alloying atomic site, so the band gap deviates strongly from the alloy-averaged properties. These results offer insights into the unique optoelectronic properties of semiconductor alloys with dissimilar band-edge wavefunction characters and emphasize the need to account for the specific band-edge wavefunction character differences in the two endpoint materials for more dependable predictions of property trends in alloys.

DOI: 10.1103/PhysRevB.109.235205

I. INTRODUCTION

Forming semiconductor alloys is a potent approach for inducing required variations in electronic properties, encompassing band gap, effective mass, and pressure deformation potentials, among others [1–7]. Semiconductor alloys typically involve combining two or more *isovalent and isostructural* materials, and it is expected that a simple and continuous variation of material properties is associated with the alloys. This has been often confirmed experimentally. For instance, (i) the unit-cell volume and lattice parameter of an alloy exhibit a nearly linear dependence on composition, adhering to Vegard's rule [8], and (ii) the band gap often demonstrates a quadratic relationship with the concentration [9].

Such schemes, despite their phenomenological nature, have proven to be a convenient and reliable tool for making practical predictions regarding the structure and electronic properties of a broad range of conventional alloys, such as (Al, Ga)(As, Sb), (Zn, Cd)(Se, Te), and Cu(In, Ga)Se_2 alloys. Nevertheless, they face challenges in understanding the electronic structure evolution in certain alloys, such as $(Al, Cr)_2O_3$ [10], $(Cr, Fe)_2O_3$ [11], (Ni, Mg)O [12], (Pb, Cd)Te [13,14], and (Co, Cu, Mg, Ni, Zn)O [15]. In these cases, experimental evidence reveals notable discontinuities in the electronic structures. These findings prompt fundamental questions: why do the electronic structures of most conventional alloys exhibit continuous variation with alloy composition while others do not? What is the underlying physical origin responsible for this phenomenon? It is important to understand the origin of these unusual variations in order to carry out material property engineering through alloying.

To address these questions, we focus on a prototype system, namely, corundum alloys α-$(Ga, M)_2O_3$, which have recently garnered great attention due to their appealing physical properties and promising potential for applications in optics, electronics, and energy [16–23]. As is known, both α-$(Ga, Al)_2O_3$ [16] and α-$(Ga, In)_2O_3$ [24,25] show conventional band-gap bowing behaviors. In this work, we take α-$(Rh_xGa_{1-x})_2O_3$ as a model alloy and conduct a systematic study of its structure and electronic properties using hybrid first-principles calculations. We find that the dependence of band gap on composition follows a discontinuous trend rather than the commonly observed quadratic function. Specifically, the band gap initially experiences an abrupt drop upon introducing a certain amount of Rh into Ga_2O_3, followed by a linear decrease with increasing Rh composition, corresponding to the evolution of wavefunction characters at the band edges. In essence, the unconventional discontinuity in the evolution of electronic properties can be attributed to the dissimilarity of the wavefunction characteristics of the band-edge states in the parent compounds. In a more general context, our research showcases a fundamental difference between conventional alloys with similar band-edge

*suhuaiwei@csrc.ac.cn
†hxdeng@semi.ac.cn

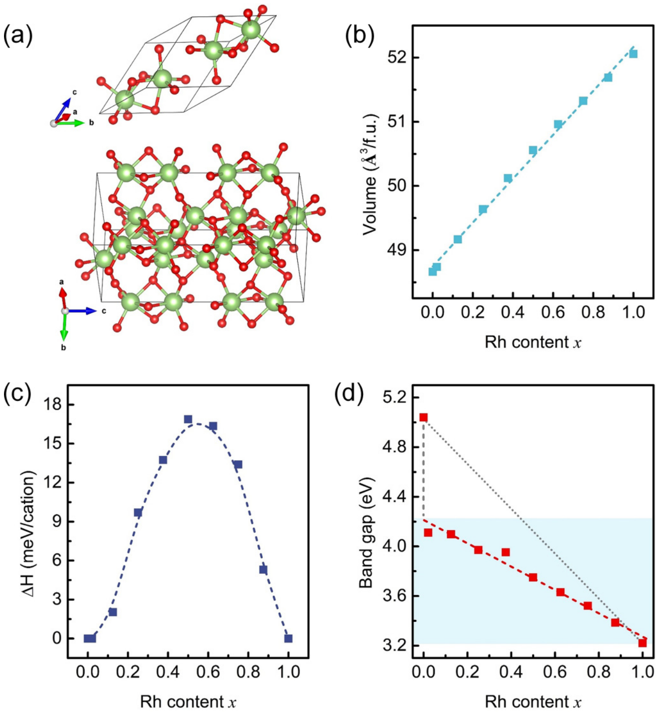

FIG. 1. (a) Primitive and hexagonal unit cells of corundum α-Ga_2O_3 (or α-Rh_2O_3). Green- and red-colored spheres represent Ga (or Rh) and O atoms, respectively. (b) Volume per formula unit, (c) mixing enthalpy per cation, and (d) band-gap energy of corundum $(Rh_xGa_{1-x})_2O_3$ alloys as a function of Rh content x. In (d), the gray dashed indicates a discontinuous band-gap change. For comparison, the fictitious linear tendency between the two endpoint binary constituents is also plotted by the gray dotted line.

wavefunction characters of the parent compounds (referred to as SBW-alloys) and alloys featuring dissimilar band-edge wavefunction characters (referred to as DBW-alloys). We explain why DBW-alloys tend to exhibit a discontinuous trend in their band gap as opposed to the common quadratic relationship observed in SBW-alloys.

II. COMPUTATIONAL METHOD

Our first-principles calculations are conducted using the projector augmented-wave method [26] and density-functional theory as implemented in the Vienna *Ab initio* Simulation Package (VASP) [27]. We set the cutoff energy to 520 eV for the plane-wave basis set. Structure optimization is performed utilizing the revised Perdew-Burke-Ernzerhof functional for solids within the generalized gradient approximation [28], and the convergence criterion of Hellmann-Feynman force on each atom is set to be 0.02 eV/Å. We sample the Brillouin zone of the 10-atom primitive cell of α-Ga_2O_3 and α-Rh_2O_3 using a Γ-centered $6 \times 6 \times 6$ Monkhorst-Pack k mesh. The primitive and hexagonal unit cells of corundum α-Ga_2O_3 or α-Rh_2O_3, with the space group of $R\bar{3}\,c$ (No. 167), are depicted in Fig. 1(a). As shown in Table I, the calculated lattice constants of both compounds exhibit good agreement with the experimental values. We calculated the electronic structures using the Heyd-Scuseria-Ernzerhof (HSE) hybrid functional [29], with a Hartree-Fock exchange parameter α of 34%. This choice produces band gaps of 5.0 and 3.4 eV for α-Ga_2O_3 and α-Rh_2O_3, respectively, in line with the experimental data (see Table I). The coincidence of the optimal mixing parameter α for both end compounds provides a rationale for favoring α-Rh_2O_3 over alternative α-M_2O_3 oxides, such as α-Ir_2O_3. We also list the two different cation–O bond lengths in each octahedron for these two compounds in Table I. The shorter (R_1) and longer (R_2) bond lengths correspond to the oxygens of the unshared and shared faces of the octahedron [30], respectively. The close bond lengths and similar lattice constants between Ga_2O_3 and Rh_2O_3 indicates that Ga_2O_3-Rh_2O_3 is a size-matched system.

We construct the random α-$(Rh_xGa_{1-x})_2O_3$ alloys using the special quasirandom structures (SQS) method [34] as implemented in the Alloy Theoretic Automated Toolkit (ATAT) [35,36]. The alloy is modeled by occupying the cation sites with Rh and Ga atoms in a 120-atom supercell (constructed by $2 \times 2 \times 1$ 30-atom unit cells), wherein the atomic correlation functions match those of the infinite fully random alloy. In this study, we simulate $(Rh_xGa_{1-x})_2O_3$ alloys with Rh compositions ranging from $x = 0\%$ (Ga_2O_3) to 100% (Rh_2O_3). Specifically, the Rh compositions investigated are 0, 2.08, 12.5, 25, 37.5, 50, 62.5, 75, 87.5, and 100%, corresponding, respectively, to the replacement of 0, 1, 6, 12, 18, 24, 30, 36, 42, and 48 Ga atoms by Rh in the 120-atom Ga_2O_3 supercell. The atomic positions of the SQS cells are fully relaxed using a Γ-centered $2 \times 2 \times 2$ Monkhorst–Pack k mesh. The band alignment between α-Ga_2O_3 and each α-$(Rh_xGa_{1-x})_2O_3$ alloys with different Rh content x is obtained by employing the standard band-offset calculation approach described in Ref. [37], following the procedure of core-level photoemission spectroscopy measurements [38].

TABLE I. Calculated lattice parameters (a, c), band gap (E_g), and bond length (R_1, R_2) of α-Ga_2O_3 and α-Rh_2O_3. Experimental values for lattice parameters and band gaps are listed in the brackets.

	a (Å)	c (Å)	E_g (eV)	Bond length (Å)
α-Ga_2O_3	5.004 (4.983[a])	13.471 (13.433[a])	5.04 (5.0[b])	$R_1 = 1.932$, $R_2 = 2.081$
α-Rh_2O_3	5.109 (5.108[c])	13.819 (13.810[c])	3.22 (3.4[d])	$R_1 = 2.021$, $R_2 = 2.057$

[a]Reference [30].
[b]Reference [31].
[c]Reference [32].
[d]Reference [33].

III. RESULTS AND DISCUSSION

Figure 1(b) illustrates the calculated alloy volume per formula unit as a function of Rh content x in the $(Rh_xGa_{1-x})_2O_3$ alloy. It is observed that the alloy volume exhibits a linear increasing trend with the concentration x, adhering to Vegard's law [8] across the whole concentration range. The mixing enthalpy (ΔH) of the $(Rh_xGa_{1-x})_2O_3$ alloy is generally written as

$$\Delta H(x) = E(Rh_xGa_{1-x}O_2) - (1-x)E(Ga_2O_3) - xE(Rh_2O_3), \quad (1)$$

where $E(Ga_2O_3)$, $E(Rh_2O_3)$, and $E(Rh_xGa_{1-x}O_2)$ represent the total energies of corundum α-Ga_2O_3, α-Rh_2O_3, and α-$(Rh_xGa_{1-x})_2O_3$ alloy, respectively. As shown in Fig. 1(c), while the mixing enthalpies are all positive, they demonstrate relatively low values. Generally, the mixing enthalpy tends to be described by a quadratic function, given by $\Delta H(x) = \Omega x(1-x)$, where Ω is the interaction parameter [39]. Here, Ω is found to be about 68 meV per cation. As a result, the maximum transition temperature $T_C = \Omega/2k_B$ is estimated to be ~394 K, suggesting that the alloying of Rh_2O_3 into Ga_2O_3 is highly probable across the entire concentration range.

For isovalent and isostructural semiconductors alloys A_xB_{1-x}, the band gap $E_g(x)$ is commonly described by the empirical expression that incorporates a quadratic bowing coefficient [9]:

$$E_g(x) = xE_g(A) + (1-x)E_g(B) - bx(1-x). \quad (2)$$

Here, $E_g(A)$ and $E_g(B)$ are the band gaps of the endpoint semiconductors A and B, respectively. The quadratic bowing coefficient, denoted as b, is a nearly constant parameter that remains independent of the composition for most isovalent semiconductor alloys except for those with large size and chemical mismatch [40]. It is important to note that the quadratic fitting is a widely accepted and utilized tool to predict the band gaps of various SBW-alloys with varying composition. However, it does not capture the behavior observed in this case. Figure 1(d) depicts the evolution of the band gap of $(Rh_xGa_{1-x})_2O_3$ alloys with regard to Rh content. In the calculation, once 1 Rh is incorporated into the 120-atom Ga_2O_3 supercell to form a $(Rh_xGa_{1-x})_2O_3$ alloy with $x = 2.08\%$, a significant drop in the band-gap width emerges. For concentrations above 2.08%, the alloy's band gap exhibits a linear diminishing trend with increasing Rh concentration. The range of tunable band gaps for the alloys is indicated by the light-blue shaded region. As a comparison to this steplike band-gap dependence on composition, we present the ideal Vegard-like behavior for the alloy band gap following Eq. (2) without considering the bowing effect (i.e., $b = 0$) using the gray dotted line.

To address the underlying physical mechanism responsible for the band-gap discontinuity in the alloys, we provide the detailed projected density of states (PDOS) for both pure compounds in Fig. 2. We analyze the wavefunctions associated with the conduction- and valence-band edges of Ga_2O_3 and Rh_2O_3, and depict the energy diagram in Fig. 2 to illustrate the relative positions and dominant characters of the band levels. The full electronic band structures of corundum Ga_2O_3 and Rh_2O_3 calculated using the HSE functional are shown in Fig. S1 of the Supplemental Material [41]. As observed in many other metal-oxide semiconductors, the valence-band maximum (VBM) state of Ga_2O_3 is primarily governed by the O $2p$ orbital, while the conduction-band minimum (CBM) is mainly comprises Ga $4s$ and O $2s$ characters. However, both the VBM and CBM of Rh_2O_3 are mainly of the Rh $4d$ characters, as reported in Ref. [42]. For reference, in the case of Rh_2O_3, we also plot the energy levels with wavefunction characters similar to those of the Ga_2O_3 band edges using dashed curves, namely p-like and s-like levels. These two levels correspond to the band-edge characters commonly observed in metal oxides. It is worth noting that if the band edges are not predominantly governed by d orbitals, as seen in common oxides, it is anticipated that the band states between two constituents hybridize and display continuous variations with respect to the alloy composition. This behavior is schematically illustrated by the dashed connecting lines in Fig. 2. In this scenario, the quadratic fitting should hold in predicting the band-gap trend.

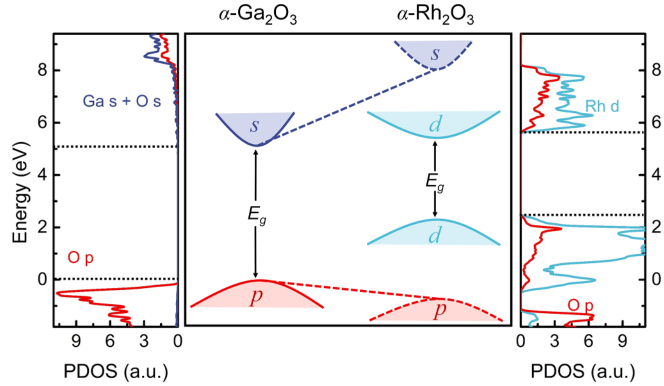

FIG. 2. Schematic energy diagrams illustrating the relative location of the conduction- and valence-band edges for the two endpoint semiconductors (solid curves in the middle panel). For Rh_2O_3, the energy level dominated by the same wavefunction characters as the Ga_2O_3 band edges are depicted by dashed curves. The dominant orbital contribution for each energy level is marked. The far left and far right panels show the calculated partial density of states of Ga_2O_3 and Rh_2O_3 binary compounds, respectively. The VBM of Ga_2O_3 ($x = 0$) is set at zero energy.

In what follows, we examine the evolution of conduction- and valence-band edge states, as well as the corresponding atomic orbital contributions, with varying Rh content in the $(Rh_xGa_{1-x})_2O_3$ alloys (see Fig. 3).

(i) VBM states: Incorporation of certain amounts of Rh into Ga_2O_3 introduces deep levels positioned above the VBM due to the higher energy level of the Rh $4d$ orbital compared to the O $2p$ orbital. This leads to a steplike increase in the energy of the VBM. As depicted in Fig. 3(c), the VBM states of the alloy are predominantly governed by Rh d orbitals as the Rh concentration surpasses 2.08%. As the Rh concentration increases, the broadening of the defect-like level facilitates an upward shift of the alloy's VBM, displaying a consistent and monotonic increasing trend.

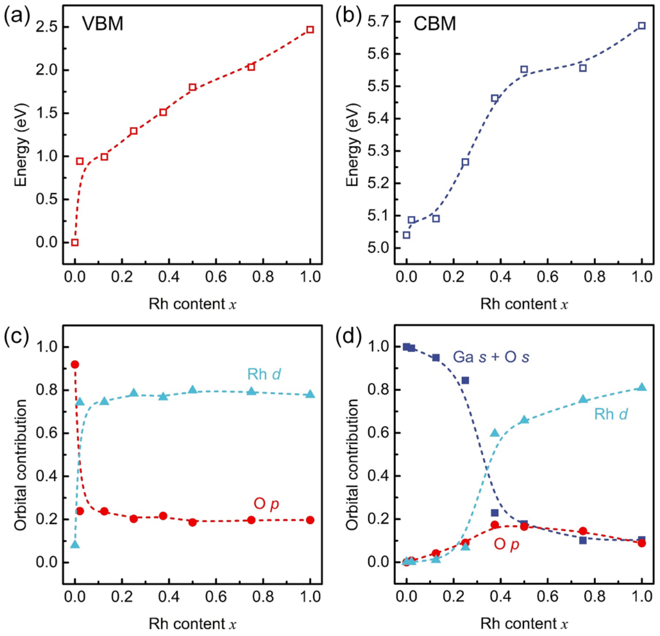

FIG. 3. Calculated band-edge positions [(a) for VBM, (b) for CBM] and the corresponding atomic orbital contribution [(c) for VBM, (d) for CBM] in $(Rh_xGa_{1-x})_2O_3$ alloys as a function of Rh concentration. The VBM of Ga_2O_3 ($x = 0$) is set at zero energy. Note the different energy scales in the VBM and CBM band edges.

(ii) CBM states: In the dilute Rh concentration regime, the CBM in the alloy remains primary composed of *s* orbitals, akin to pure Ga_2O_3. As the Rh concentration increases, the broadening of the Rh *d* orbital enables increased contributions to the CBM of the alloy, resulting in a steep upward trend in the energy of the CBM. As the Rh composition increases, the decreasing contribution of *s* orbitals and the increasing contribution of *d* orbitals results in a crossover at a critical Rh composition (∼0.35). With further increase in Rh composition, the Rh *d* orbitals gradually dominate the CBM, similar to pure Rh_2O_3, causing the variation of the CBM to slow down.

The VBM shows a much larger variation range compared to the CBM, resulting in the band-gap evolution being primarily influenced by the VBM trend, leading to a steplike decreasing pattern as shown in Fig. 1(d). To demonstrate the evolution in the dispersion of the Rh *d* states and their impact on the band gap, we also offer a plot illustrating the evolution of the partial density of states (PDOS) for $(Rh_xGa_{1-x})_2O_3$ alloys with distinct x values of 0, 2.08, 25, 50, 75, and 100%, where each band gap is indicated, as depicted in Fig. S2 of the Supplemental Material [41]. Additionally, to understand the alloy's optoelectronic properties and further validate the role of Rh *d* states in the formation of the alloy's VBM, we examine the optical absorption coefficients of $(Rh_xGa_{1-x})_2O_3$ alloys as a function of Rh concentration (see Fig. S3 in the Supplemental Material [41]). Notably, upon adding 1 Rh atom into the Ga_2O_3 supercell ($x = 2.08\%$), the optical absorption threshold significantly drops. With increasing Rh concentration, the optical absorption threshold gradually diminishes, falling in line with the electronic band-gap trend.

One shall want to know for the alloys with low Rh concentration, specifically at 2.08% (i.e., 1 Rh in the 120-atom cell), whether the energy difference between the Rh *d*-related highest occupied and lowest unoccupied states (HOMO-LUMO) corresponds just to a diminished optical absorption threshold, or to a narrowed mobility gap [43]. At $x = 2.08\%$, there is 1 Rh atom in the 120-atom supercell with a volume of 1169.74 Å^3. Since each Rh contributes 3 *d*-states, the concentration of Rh *d* states is $\sim 2.6 \times 10^{21}$ cm^{-3}, which is about one order of magnitude larger than the effective number of states of the VBM ($\sim 1.3 \times 10^{20}$ cm^{-3}) for α-Ga_2O_3 (calculated with a hole effective mass of $\sim 3m_0$ at room temperature). Besides, from Fig. S2 of the Supplemental Material, it is observed that the 2.08% Rh composition forms a VB band with relatively high density of states. Consequently, the band of Rh *d*-related occupied states can be regarded as the highest VB of the alloy. Given that the CB shift for low Rh concentrations is relatively small, the designation of the Rh *d*-related HOMO-LUMO difference as a (mobility) band gap is credible.

The above analysis of the composition-dependent optoelectronic properties in α-$(Rh_xGa_{1-x})_2O_3$ underscores that the virtual crystal approximation is not suitable for DBW-alloys. This is due to the fact that the continuous Vegard-like scheme is derived from conventional SBW-alloys [9,44–46], where the alloy wavefunction is delocalized over the whole region, allowing for a proper alloy average. *However, in DBW-alloys, the band-edge wavefunction is localized on a specific atomic site, rendering the alloy average inappropriate.* With this understanding, the experimentally observed discontinuous band-gap variations in α-$(Al_xCr_{1-x})_2O_3$ [10], akin to those in the α-$(Rh_xGa_{1-x})_2O_3$ alloy, can be readily understood. Additionally, it is essential to acknowledge the potential concerns regarding the accuracy of band-gap trends and band-edge positions estimated through the quadratic fitting in a recent investigation of $(Ir_xGa_{1-x})_2O_3$ alloy [23].

Given the inapplicability of the virtual crystal approximation in DBW-alloys and the laborious nature of measuring alloy properties across a densely populated mesh of compositions, adopting more refined theoretical frameworks for studying alloy properties is imperative to avoid overlooking irregularities in physical properties for semiconductor alloys. From a theoretical standpoint, it is essential to initially consider the specific band-edge wavefunction characters in the two endpoint materials before commencing alloy calculations. For DBW-alloys with dissimilar band-edge wavefunction characters, it is recommended to conduct calculations focusing on the dilute composition limit ($x \to 0$ or $x \to 1$) utilizing a relatively large supercell. By combining these calculations with data from common compositions, such as $x = 0$, 25, 50, 75, and 100%, a reliable prediction of property trends within DBW-alloys can be achieved.

IV. CONCLUSION

To conclude, we have performed first-principles calculations to study the structural and optoelectrical properties of the α-$(Rh_xGa_{1-x})_2O_3$ alloy, aiming to elucidate the physical origin responsible for the discontinuous band-gap dependence on composition in certain alloys. We find that the band gap undergoes a steplike and discontinuous variation with changing Rh composition, which correlates with the evolution of wavefunction characters in the band edges. These findings give a detailed picture for the electronic structure evolution within the α-$(Rh_xGa_{1-x})_2O_3$ alloy, emphasizing that DBW-alloys often manifest a discontinuous trend in their electronic structures, in contrast to the typical quadratic relationship observed in SBW-alloys. Our study provides guidance for future research in similar alloy systems, facilitating accurate predictions of the alloy properties.

ACKNOWLEDGMENTS

This work was supported by the National Natural Science Foundation of China (Grants No. 12204471, No. 11991060, No. 12088101, No. U2230402, and No. 12104181), the Strategic Priority Research Program of the Chinese Academy of Sciences (Grant No. XDB0460000), the National Key Research and Development Program of China (Grant No. 2020YFB1506400), and the Jilin Scientific and Technological Development Program (Grant No. 20210101162JC).

[1] D. G. Thomas, J. J. Hopfield, and C. J. Frosch, Isoelectronic traps due to nitrogen in gallium phosphide, Phys. Rev. Lett. **15**, 857 (1965).

[2] J. A. Van Vechten and T. K. Bergstresser, Electronic structures of semiconductor alloys, Phys. Rev. B **1**, 3351 (1970).

[3] H. P. Hjalmarson, P. Vogl, D. J. Wolford, and J. D. Dow, Theory of substitutional deep traps in covalent semiconductors, Phys. Rev. Lett. **44**, 810 (1980).

[4] S.-H. Wei and A. Zunger, Band gaps and spin-orbit splitting of ordered and disordered $Al_xGa_{1-x}As$ and $GaAs_xSb_{1-x}$ alloys, Phys. Rev. B **39**, 3279 (1989).

[5] S. Adachi, *Properties of Semiconductor Alloys: Group-IV, III-V and II-VI Semiconductors* (John Wiley & Sons, New Jersey, 2009).

[6] H.-X. Deng, J. Li, S.-S. Li, H. Peng, J.-B. Xia, L.-W. Wang, and S.-H. Wei, Band crossing in isovalent semiconductor alloys with large size mismatch: First-principles calculations of the electronic structure of Bi and N incorporated GaAs, Phys. Rev. B **82**, 193204 (2010).

[7] X. Cai, F. P. Sabino, A. Janotti, and S.-H. Wei, Approach to achieving a *p*-type transparent conducting oxide: Doping of bismuth-alloyed Ga_2O_3 with a strongly correlated band edge state, Phys. Rev. B **103**, 115205 (2021).

[8] L. Vegard, Die konstitution der mischkristalle und die raumfüllung der atome, Z. Phys. **5**, 17 (1921).

[9] J. E. Bernard and A. Zunger, Electronic structure of ZnS, ZnSe, ZnTe, and their pseudobinary alloys, Phys. Rev. B **36**, 3199 (1987).

[10] R. Jangir, V. Srihari, A. Bhakar, C. Kamal, A. K. Yadav, P. R. Sagdeo, D. Kumar, S. Tripathi, S. N. Jha, and T. Ganguli, Structural and optical properties of transparent, tunable bandgap semiconductor: α-$(Al_xCr_{1-x})_2O_3$, J. Appl. Phys. **128**, 135703 (2020).

[11] S. E. Chamberlin, Y. Wang, K. Lopata, T. C. Kaspar, A. W. Cohn, D. R. Gamelin, N. Govind, P. V. Sushko, and S. A. Chambers, Optical absorption and spectral photoconductivity in α-$(Fe_{1-x}Cr_x)_2O_3$ solid-solution thin films, J. Phys.: Condens. Matter **25**, 392002 (2013).

[12] C. A. Niedermeier, M. Råsander, S. Rhode, V. Kachkanov, B. Zou, N. Alford, and M. A. Moram, Band gap bowing in $Ni_xMg_{1-x}O$, Sci. Rep. **6**, 31230 (2016).

[13] P. M. Nikolic, Solid solutions of CdSe and CdTe in PbTe and their optical properties, Br. J. Appl. Phys. **17**, 341 (1966).

[14] E. I. Rogacheva, Critical phenomena in heavily-doped semiconducting compounds, Jpn. J. Appl. Phys. **32**, 775 (1993).

[15] N. J. Usharani, P. Arivazhagan, T. Thomas, and S. S. Bhattacharya, Factors determining the band gap of a nanocrystalline multicomponent equimolar transition metal based high entropy oxide (Co, Cu, Mg, Ni, Zn)O, Mater. Sci. Eng. B **283**, 115847 (2022).

[16] H. Ito, K. Kaneko, and S. Fujita, Growth and band gap control of corundum-structured α-$(AlGa)_2O_3$ thin films on sapphire by spray-assisted mist chemical vapor deposition, Jpn. J. Appl. Phys **51**, 100207 (2012).

[17] Y. L. Kim, Y. Ha, N.-S. Lee, J. G. Kim, J. M. Baik, C. Lee, K. Yoon, Y. Lee, and M. H. Kim, Hybrid architecture of rhodium oxide nanofibers and ruthenium oxide nanowires for electrocatalysts, J. Alloys Compd. **663**, 574 (2016).

[18] J. Bai, S.-H. Han, R.-L. Peng, J.-H. Zeng, J.-X. Jiang, and Y. Chen, Ultrathin rhodium oxide nanosheet nanoassemblies: Synthesis, morphological stability, and electrocatalytic application, ACS Appl. Mater. Interfaces **9**, 17195 (2017).

[19] Q. Feng, X. Li, G. Han, L. Huang, F. Li, W. Tang, J. Zhang, and Y. Hao, $(AlGa)_2O_3$ solar-blind photodetectors on sapphire with wider bandgap and improved responsivity, Opt. Mater. Express **7**, 1240 (2017).

[20] S.-i. Kan, S. Takemoto, K. Kaneko, I. Takahashi, M. Sugimoto, T. Shinohe, and S. Fujita, Electrical properties of α-Ir_2O_3/α-Ga_2O_3 *pn* heterojunction diode and band alignment of the heterostructure, Appl. Phys. Lett. **113**, 212104 (2018).

[21] K. Kaneko, S. Fujita, and T. Hitora, A power device material of corundum-structured α-Ga_2O_3 fabricated by MIST EPITAXY® technique, Jpn. J. Appl. Phys. **57**, 02CB18 (2018).

[22] J. G. Hao, H. H. Gong, X. H. Chen, Y. Xu, F. F. Ren, S. L. Gu, R. Zhang, Y. D. Zheng, and J. D. Ye, *In situ* heteroepitaxial construction and transport properties of lattice-matched α-Ir_2O_3/α-Ga_2O_3 p-n heterojunction, Appl. Phys. Lett. **118**, 261601 (2021).

[23] K. Kaneko, Y. Masuda, S.-i. Kan, I. Takahashi, Y. Kato, T. Shinohe, and S. Fujita, Ultra-wide bandgap corundum-structured *p*-type α-$(Ir, Ga)_2O_3$ alloys for α-Ga_2O_3 electronics, Appl. Phys. Lett. **118**, 102104 (2021).

[24] N. Suzuki, K. Kaneko, and S. Fujita, Growth of corundum-structured $(In_xGa_{1-x})_2O_3$ alloy thin films on sapphire substrates with buffer layers, J. Cryst. Growth **401**, 670 (2014).

[25] J. E. N. Swallow, R. G. Palgrave, P. A. E. Murgatroyd, A. Regoutz, M. Lorenz, A. Hassa, M. Grundmann, H. von Wenckstern, J. B. Varley, and T. D. Veal, Indium gallium oxide alloys: Electronic structure, optical gap, surface space charge, and chemical trends within common-cation semiconductors, ACS Appl. Mater. Interfaces **13**, 2807 (2021).

[26] G. Kresse and D. Joubert, From ultrasoft pseudopotentials to the projector augmented-wave method, Phys. Rev. B **59**, 1758 (1999).

[27] G. Kresse and J. Furthmüller, Efficient iterative schemes for *ab initio* total-energy calculations using a plane-wave basis set, Phys. Rev. B **54**, 11169 (1996).

[28] J. P. Perdew, A. Ruzsinszky, G. I. Csonka, O. A. Vydrov, G. E. Scuseria, L. A. Constantin, X. Zhou, and K. Burke, Restoring the density-gradient expansion for exchange in solids and surfaces, Phys. Rev. Lett. **100**, 136406 (2008).

[29] J. Heyd, G. E. Scuseria, and M. Ernzerhof, Hybrid functionals based on a screened Coulomb potential, J. Chem. Phys. **118**, 8207 (2003).

[30] M. Marezio and J. P. Remeika, Bond lengths in the α-Ga_2O_3 structure and the high-pressure phase of $Ga_{2-x}Fe_xO_3$, J. Chem. Phys. **46**, 1862 (1967).

[31] V. D. Wheeler, N. Nepal, D. R. Boris, S. B. Qadri, L. O. Nyakiti, A. Lang, A. Koehler, G. Foster, S. G. Walton, and C. R. Eddy Jr, Phase control of crystalline Ga_2O_3 films by plasma-enhanced atomic layer deposition, Chem. Mater. **32**, 1140 (2020).

[32] A. Wold, R. J. Arnott, and W. J. Croft, The reaction of rare earth oxides with a high temperature form of rhodium (III) oxide, Inorg. Chem. **2**, 972 (1963).

[33] J. Ghose and A. Roy, Optical studies on Rh_2O_3, AIP Conf. Proc. **370**, 901 (1996).

[34] S. H. Wei, L. G. Ferreira, J. E. Bernard, and A. Zunger, Electronic properties of random alloys: Special quasirandom structures, Phys. Rev. B **42**, 9622 (1990).

[35] A. Van De Walle, M. Asta, and G. Ceder, The alloy theoretic automated toolkit: A user guide, Calphad **26**, 539 (2002).

[36] A. Van De Walle and G. Ceder, Automating first-principles phase diagram calculations, J. Phase Equilib. **23**, 348 (2002).

[37] S. H. Wei and A. Zunger, Valence band splittings and band offsets of AlN, GaN, and InN, Appl. Phys. Lett. **69**, 2719 (1996).

[38] G. Martin, S. Strite, A. Botchkarev, A. Agarwal, A. Rockett, H. Morkoc, W. R. L. Lambrecht, and B. Segall, Valence-band discontinuity between GaN and AlN measured by *x*-ray photoemission spectroscopy, Appl. Phys. Lett. **65**, 610 (1994).

[39] Y.-F. Zheng, L. Huang, B. Li, R. Wang, and S.-H. Wei, Origin of the improved performance of $Cu(In,Ga)(S, Se)_2$ solar cells by postdeposition treatments: Effect of band offsets, Phys. Rev. Appl. **15**, 064036 (2021).

[40] S.-H. Wei and A. Zunger, Giant and composition-dependent optical bowing coefficient in GaAsN alloys, Phys. Rev. Lett. **76**, 664 (1996).

[41] See Supplemental Material at http://link.aps.org/supplemental/10.1103/PhysRevB.109.235205 for the calculated band structures of Ga_2O_3 and Rh_2O_3, as well as the total and partial density of states and the optical absorption coefficients of $(Rh_xGa_{1-x})_2O_3$ alloys.

[42] X. Cai, S.-H. Wei, P. Deák, C. Franchini, S.-S. Li, and H.-X. Deng, Band-gap trend of corundum oxides α-M_2O_3 ($M =$ Co, Rh, Ir): An *ab initio* study, Phys. Rev. B **108**, 075137 (2023).

[43] V. K. Gupta, M. Lorke, T. Frauenheim, and P. Deák, Possibilities and limits of decreasing the gap of anatase TiO_2 by alloying with nitrogen, J. Phys. Chem. C **125**, 3192 (2021).

[44] K. A. Mäder and A. Zunger, Short-and long-range-order effects on the electronic properties of III-V semiconductor alloys, Phys. Rev. B **51**, 10462 (1995).

[45] W. J. Fan, M. F. Li, T. C. Chong, and J. B. Xia, Electronic properties of zinc-blende GaN, AlN, and their alloys $Ga_{1-x}Al_xN$, J. Appl. Phys. **79**, 188 (1996).

[46] M. V. Fischetti and S. E. Laux, Band structure, deformation potentials, and carrier mobility in strained Si, Ge, and SiGe alloys, J. Appl. Phys. **80**, 2234 (1996).